

Evaluation of high-strength cementitious composite with iron ore tailing and gneiss waste as mineral admixture

Avaliação de compósito cimentício de alta resistência com rejeito de minério de ferro e resíduo de gnaissse como adições minerais

¹Abner Araújo Fajardo

¹Universidade Federal de Minas Gerais
Belo Horizonte - MG - Brazil

²Silvia Roberta Souza

²Universidade Federal de Minas Gerais
Belo Horizonte - MG - Brazil

³Dyala Fraga do Prado

³Universidade Federal de Minas Gerais
Belo Horizonte - MG - Brazil

⁴Jordana Gonçalves de Macedo

⁴Universidade Federal de Minas Gerais
Belo Horizonte - MG - Brazil

⁵Vinicius Ferreira Lanna

⁵Universidade Federal de Minas Gerais
Belo Horizonte - MG - Brazil

⁶Maria Teresa Paulino Aguiar

⁶Universidade Federal de Minas Gerais
Belo Horizonte - MG - Brazil

⁷Dayana Cristina Silva Garcia

⁷Universidade Federal de Minas Gerais
Belo Horizonte - MG - Brazil

⁸Maria Teresa Gomes Barbosa

⁸Universidade Federal de Juiz de Fora
Juiz de Fora - MG - Brazil

⁹Fernando do Couto Rosa Almeida

⁹Universidade Federal de Minas Gerais
Belo Horizonte - MG - Brazil

¹⁰White José dos Santos

¹⁰Universidade Federal de Minas Gerais
Belo Horizonte - MG - Brazil

Recebido em 27/01/25
Aceito em 27/05/25


Abner Araújo Fajardo 

Silvia Roberta Souza 

Dyala Fraga do Prado 

Jordana Gonçalves de Macedo 

Vinicius Ferreira Lanna 

Maria Teresa Paulino Aguiar 

Dayana Cristina Silva Garcia 

Maria Teresa Gomes Barbosa 

Fernando do Couto Rosa Almeida 

White José dos Santos 

Abstract

This study aimed to evaluate the physical-mechanical properties, electrical resistivity and microstructural characteristics of high-strength cementitious composites (HSCC) incorporating iron ore tailings (IOT) and quarry residue (gneiss powder - GN) at 28 and 180 days. The results showed that IOT and GN samples exhibited high compressive strength (> 90 MPa) and flexural strength (> 6 MPa). Little difference was identified regarding the hydrated phases. In the interfacial transition zone, the IOT and GN samples presented low pore content and reduced extension. It was concluded that high-strength cementitious composites with excellent physical and mechanical and durability performance could be developed using a mixture design based on particle packing and the incorporation of IOT and GN.

Key words: Iron Ore Tailings (IOT). Gneiss waste. Mineral admixture. High-strength cementitious composite. Microstructure.

Resumo

Objetiva-se avaliar as propriedades físico-mecânicas, resistividade elétrica e características microestruturais de compósitos cimentícios de alta resistência (HSCC) com adição de rejeito de Mineração de Ferro (IOT) e resíduo de pedreiras (pó de gnaissse - GN) aos 28 e 180 dias de idade. Os resultados mostraram que as argamassas IOT e GN apresentam alta resistência à compressão (> 90 MPa) e à flexão (> 6 MPa). Pouca diferença foi identificada em relação às fases hidratadas. Na zona de transição interfacial, as amostras IOT e GN apresentaram baixo teor de poros e extensão reduzida. Conclui-se que, empregando um planejamento de mistura baseado em empacotamento de partículas, foi possível desenvolver compósitos cimentícios de alta resistência com excelente desempenho físico-mecânico e durabilidade com a adição de IOT e GN.

Palavras-chave: Rejeito de mineração de ferro. Resíduos de gnaissse. Adição mineral. Compósito cimentício de alta resistência. Microestrutura.

Introduction

The construction industry consumes approximately 30% of the world's raw materials and 25% of its available freshwater (Giannetti *et al.*, 2018). However, this sector has great potential to incorporate alternative materials, from industrial and mining waste, contributing to the reduction of the social, economic, and environmental impacts of its production (Almada *et al.*, 2022; Leão *et al.*, 2024; Torres *et al.*, 2024).

In 2022, Brazil produced approximately 640 million tons of coarse and fine aggregates by processing granitoid rocks, such as granite and gneiss (ANEPAC, 2024). The final waste product from rock crushing, a powdery material known as gneiss powder (GN) (Schankoski *et al.*, 2019), is often improperly stored outdoors, leading to environmental degradation and inefficient use of mineral resources (Chen *et al.*, 2015).

Several studies have investigated the use of gneiss powder in both conventional and self-compacting concrete production, demonstrating significant improvements in mechanical properties and durability (Chen *et al.*, 2015; Schankoski *et al.*, 2019; Yannick *et al.*, 2024). Gneiss can also be used in asphalt mixtures, where it has been shown to increase tensile strength by 22% (Chen *et al.*, 2015). Additionally, it has the potential to be used in “eco-friendly cement mortar”, where replacing 50% of cement with GN resulted in a 20% reduction in compressive strength (Yannick *et al.*, 2024).

Iron ore holds significant importance for Brazil, which ranks as the second-largest producer in the world, surpassed only by Australia. In 2020, Brazil produced approximately 400 million tons of iron ore, accounting for 66.36% of the country's total mineral production (USGS, 2021; BMI, 2021). Of this amount, 370.9 million tons were exported, generating around 36.6 billion dollars in revenue. According to the National Mining Agency (NMA, 2021), the states of Minas Gerais and Pará were responsible for 89.4% of the country's iron ore production. Iron ore tailings (IOT) are by-products of mining operations, and their disposal poses significant risks to surrounding communities and the environment (Pires *et al.*, 2019). Large volumes of IOT are stored in dams or piles, which leads to leaching processes that contaminate surface water, groundwater, and soil with heavy metals (Luo *et al.*, 2020; Cancio *et al.*, 2018). Brazil has recently faced two major dam collapse tragedies: one in Mariana (2015) and one in Brumadinho (2019). Both occurred in the state of Minas Gerais and resulted in significant loss of life and widespread environmental devastation (Cancio *et al.*, 2018; Chácara; Oliveira Filho, 2021).

The use of IOT as a fine aggregate in cementitious composites has already been well-documented in the literature (Carrasco *et al.*, 2017; Ling *et al.*, 2021; Lv *et al.*, 2021). However, the finest portion ($< 75 \mu\text{m}$) cannot be used as fine aggregate (sand). Instead, it can be used as an alternative mineral admixture. Studies have shown that pozzolanic activation of IOT is difficult, even after mineral admixture grinding and magnetic separation processes (Almada *et al.*, 2022). Several studies have reported a reduction in mechanical properties when IOT was used in cementitious binders (Cancio *et al.*, 2018; Gu *et al.*, 2022; Magalhães *et al.*, 2018; Moraes *et al.*, 2021; Ling *et al.*, 2021). However, there is limited research on its use as a mineral admixture to improve the performance of conventional mortars and concrete (Almada *et al.*, 2022, 2023; Castro *et al.*, 2021; Carvalho *et al.*, 2022). These latter authors observed increases of over 20% in mechanical and physical properties when 40% of IOT was added, compared to the reference mix. However, none of these studies have compared the results of IOT composites with those of other conventional mineral admixtures, such as GN. Moreover, there is a lack of research focusing on the finest fraction of IOT powder, especially regarding its impact on physical and mechanical properties, durability, and microstructural features.

The objective of this study is to evaluate the physical and mechanical properties, electrical resistivity, and microstructural characteristics of high-strength cementitious composites (HSCC) containing the fine portion (smaller than $75 \mu\text{m}$) of iron ore tailings (IOT) and quarry waste (gneiss powder - GN) at 28 and 180 days of age.

Materials and methods

Materials

The materials used were: ordinary Portland cement (with up to 5% limestone filler – CPV-ARI, similar to Type III cement according to C150 (ASTM, 2024); quartz sand; silica fume ($\text{SiO}_2 > 90\%$, specific surface: $20,000 \text{ m}^2/\text{kg}$, specific gravity: $2,220 \text{ kg/m}^3$ and particle diameter: 200 nm); polycarboxylate superplasticizer with normal setting time (density $1,120 \text{ kg/m}^3$); iron ore tailings (IOT); and gneiss powder (GN), with 90% passing through a $150 \mu\text{m}$ sieve (Figure 1).

Figure 1 - Illustrative images of the materials used: (a) iron ore tailings (IOT) and (b) gneiss powder (GN)



The IOT was extracted from a mine located in the Iron Quadrangle, in the state of Minas Gerais, Brazil. The silica fume, collected in bag filters, originated from the manufacturing process of metallic silicon and ferrosilicon. It was stored in suitable silos and packaged in kraft paper bags. The gneiss filler was supplied by Mineração Santiago, a company located in the Céu Azul neighborhood of Belo Horizonte, in the state of Minas Gerais. For GN, only the fraction passing through the 150 μm sieve was used. Both IOT and GN were dried at 105 °C for 24 hours

Materials characterization

Portland cement, silica fume, IOT and gneiss powder were characterized in terms of their physical, chemical and mineralogical properties, according to the procedures described below:

- (a) the chemical composition was determined by X-ray fluorescence (XRF) analysis, using lithium tetraborate fusion. Loss on ignition (LOI) was assessed by calcining the sample at 1000 °C;
- (b) the mineralogical composition was identified using X-ray diffraction (XRD), with a Philips PW 1710 instrument and $\text{CuK}\alpha$ radiation ($\lambda = 1.54 \text{ \AA}$, $V = 50 \text{ kV}$), at a step size of 0.02°/s. Phase identification was performed using the Crystallography Open Database (COD) in the HighScore Plus software;
- (c) particle size distribution was obtained using a laser diffraction granulometer, Sympatec brand model Helos 12LA, computerized with a 50 mm lens. A 0.05% sodium hexametaphosphate solution was used as dispersant. For cement analysis, isopropyl alcohol was used as a dispersant in a CILAS 1064 granulometer. The smallest measured particle diameter was 0.03 μm , and the sample was agitated in an ultrasonic bath for 60 seconds before and during the analysis. Quartz sand was analyzed by sieving (ABNT, 2015);
- (d) specific surface area (SSA) and porosity: The Brunauer, Emmett, and Teller (BET) model was used to calculate the SSA, and the Non-Local Density Functional Theory (NLDFT) model was applied for pore size distribution. The Quantachrome Nova 1200e equipment and the Quantachrome NovaWin software version 11.02 were used to determine the SSA and pore distribution of the IOT, gneiss filler and cement. The samples were previously dried under vacuum at 150 °C for 48 hours to clean the surface. Nitrogen (N_2) was used as the adsorbate, and to calculate the complete isotherm, the analysis time for each sample was 24 hours. The specific surface area was calculated using the multipoint BET adsorption isotherm, and porosity was determined using the NLDFT model applied to the desorption isotherm;
- (e) morphology and microstructure features: Scanning electron microscopy (SEM) was used to obtain micrographs of the particle shape and surface texture. The dust materials were deposited onto self-adhesive carbon tapes and gold-coated using the Quorum Q150R ES equipment. The images were acquired using a Tescan's MEV-VEGA3 SEM, which operates by thermionic emission with a tungsten filament. The samples were vacuumed for 15 minutes prior to imaging, with an accelerating voltage of 20 kV. INCA X-act energy dispersive spectrometer (EDS) from Oxford instruments, coupled to the SEM, was used to perform elemental mapping and identify the chemical elements present in the particles of the materials; and

- (f) specific gravity: The helium gas pycnometer technique was used to determine the true specific gravity of the materials. The pycnometer model used was the Quantachrome Multi Pycnometer MVP-1. The samples were kept in the oven at 70 °C for 12 hours before the test.

Mix design

Cementitious composite mixes were designed using the particle packing method with the Elkem Materials Mixture Analyzer (EMMA) software, based on the modified Andreasen and Andersen model. The input values were the largest and smallest particle sizes: 2.4 mm (sand) and 0.1 μm (IOT and cement), respectively. A distribution modulus of $q = 0.30$ was adopted, which indicates satisfactory flow capacity (Almada *et al.*, 2022; ABNT, 2019). The 1:3 cement-to-sand mixture showed the best packing performance when combined with 25% silica fume and 40% IOT or gneiss powder (by cement mass). The water-to-cement ratio (w/c) was set at 0.375, and the amount of superplasticizer was adjusted to achieve a target consistency of 230 ± 10 mm on the flow table (Figure 2).

The amount of raw materials used in the composites is shown in Table 1. The raw materials were mixed in an inclined shaft concrete mixer, following this sequence: sand, silica fume, cement, IOT and GN; followed by half of the mixing water; and then the remaining water along with the superplasticizer. The fresh mixtures were cast into metallic molds (cubic, prismatic and cylindrical) and compacted on a vibrating table for one minute. After 24 hours, the specimens were demolded and cured in water until the testing ages of 28 and 180 days.

Characterization of high-strength cementitious composite

Compressive strength was determined based on the average of five cubic specimens ($5 \times 5 \times 5 \text{ cm}^3$) (ABNT, 2019), using an EMIC Universal Testing Machine (model DL2000) with a loading speed of (0.45 ± 0.15) MPa/s. Flexural strength was determined using the average of three prismatic specimens ($4 \times 4 \times 16 \text{ cm}^3$) (ABNT, 2005a), with the same EMIC DL2000 equipment and a loading speed at (1.00 ± 0.15) MPa/s. Water absorption by capillary rise (ABNT, 2012), water absorption by total immersion, open porosity and specific gravity (ABNT, 2005b) were determined based on the average results of four cylindrical specimens ($\phi 5 \times 10 \text{ cm}^2$), measured with a precision scale with 0.01g accuracy.

Volumetric and surface electrical resistivity tests were performed on cylindrical samples ($\phi 10 \times 20 \text{ cm}^2$), using the PROCEQ Resipod. The equipment features four pins that make contact with the sample surface. A current is applied through the two outer pins, while the resulting potential difference is measured across the two inner pins (ASTM, 2019). Prior the test, the specimens were kept immersed in water for 72 hours.

Figure 2 - Illustrative images showing the flow of mortars containing (a) IOT and (b) GN

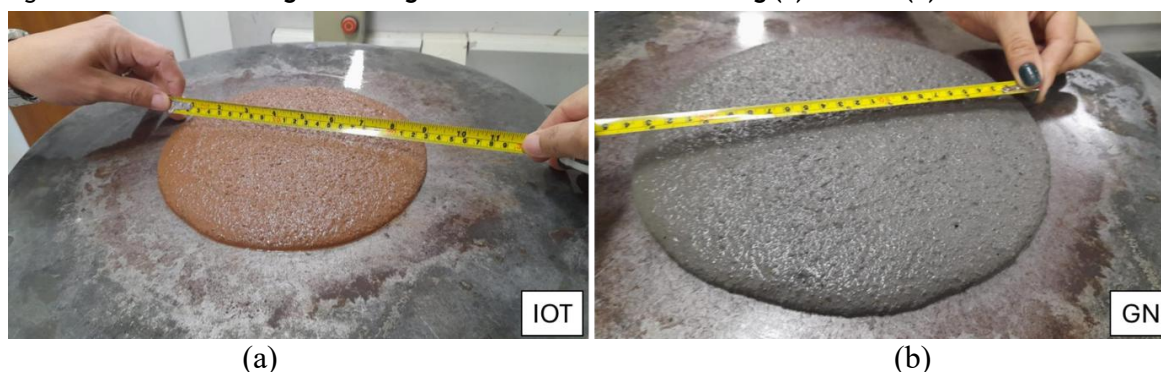


Table 1 - Quantity of raw materials for the production of mixtures

Sample	Cement (kg/m^3)	Sand (kg/m^3)	Silica Fume (kg/m^3)	IOT (kg/m^3)	GN (kg/m^3)	Water (kg/m^3)	Superplasticizer (kg/m^3)
Ref.	507	1520	127	0	0	190	10
IOT	479	1437	120	192	0	180	14
GN	469	1407	117	0	188	176	14

Microstructural analysis was performed using SEM-EDS to quantify hydrated and unhydrated compounds, as well as to evaluate the width of the Interfacial Transition Zone (ITZ). Samples were coated with a 15 nm layer of carbon and subjected to analysis using a FEI Quanta 3D scanning electron microscope. Images were obtained in backscattered electron mode, with an acceleration voltage of 20 kV and a working distance of 10 mm. ImageJ software was used for binary segmentation and phase analysis (CH, anhydrous cement, C-S-H), and their distribution on the micrographs. Three fragments per sample were tested, and at least 20 micrographs of each fragment were analyzed to determine the number of pores and anhydrous phases.

Thermogravimetric analysis was carried out using a Shimadzu thermal analyzer (model TGA-51) under a nitrogen atmosphere, with a flow rate of 50 mL/min. The temperature ranged from 25 °C to 1000 °C, with a heating rate of 10 °C/min. This test aimed to quantify the contents of calcium hydroxide and calcium carbonate.

Results and discussion

Materials characterization

The particle size distribution of the raw materials is shown in Figure 3 and Table 2. The average particle size of gneiss powder (GN) was 39.90 μm , which is larger than that of the iron ore tailing (IOT), with an average of 4.70 μm . The IOT result is similar to those reported in the literature: Chinese studies: 5.00 μm – 10.00 μm (Liu *et al.*, 2019), 5.00 μm (Huang; Ranade; Li, 2013) and 2.76 μm (Guang; Deng; Wang, 2014); and Brazilian authors - 0.61 μm (Cancio *et al.*, 2018), 0.86 μm (Carvalho *et al.*, 2022) and 0.86 μm (Magalhães *et al.*, 2018).

Figure 3 - Accumulated particle size distribution of cement, silica fume, IOT, GN and sand

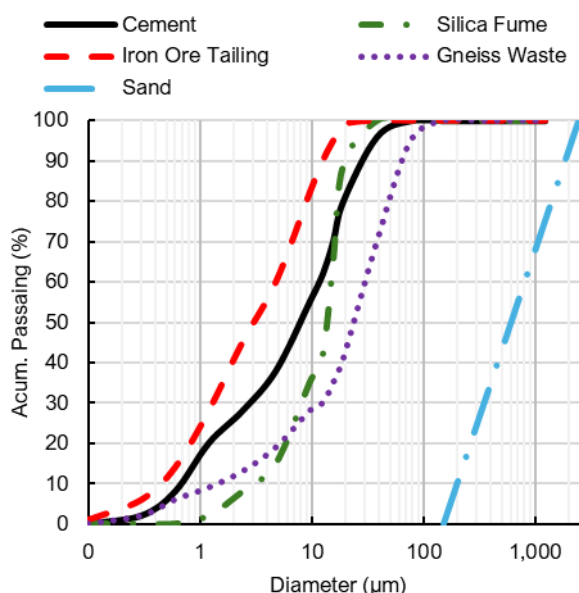


Table 2 - Physical properties of the materials

Physical properties	Diameter	Silica fume	IOT	GN	Cement
Particle size (μm)	D ₁₀	3.76	0.43	3.28	7.30
	D ₅₀	13.74	3.63	32.62	28.00
	D ₉₀	24.41	12.90	87.79	47.00
Specific gravity (g/cm^3)		2.20	3.84	2.70	3.12
Specific surface area (m^2/g)		22,010	35,113	2,240	1,743
Pore Volume ($10^{-3} \text{ cm}^3/\text{g}$)		1.901	0.5712	6.725	5.896

The IOT showed the highest specific surface area value (35,113 m²/g), followed by the silica fume (22,010 m²/g), the gneiss powder (2,240 m²/g) and the Portland cement (1,743 m²/g). The SSA value of the IOT is significantly higher than those reported other studies: 29,547 m²/g (Carvalho *et al.*, 2022), 10,107 m²/g (Almada *et al.*, 2023), 6,020 m²/g (Castro *et al.*, 2021), 2,030 m²/g (Cheng *et al.*, 2016), 1,185 m²/g (Zhang *et al.*, 2020) and 1,735 m²/g (Bezerra *et al.*, 2021). This indicates that the IOT used in the present study is considerably finer than the tailings used by other authors. Furthermore, the IOT had the lowest total pore volume (0.571x10⁻³ cm³/g) among the raw materials analyzed, followed by the silica fume (1.901x10⁻³ cm³/g), the Portland cement (5.896x10⁻³ cm³/g) and the gneiss powder (6.725x10⁻³ cm³/g) (Table 1). This may be due to the presence of finer particles in the IOT and the silica fume that were not detected by the particle size analyzer, thus contributing to the higher SSA values observed.

The GN exhibited a density 30.59% lower than that of the IOT waste, due to differences in their chemical compositions, as shown in Table 3. The IOT is primarily composed of iron (48.00%) and silicon (21.20%) oxides. On the other hand, GN mainly consists of silicon (70.50%) and aluminum (14.30%) oxides. The silica fume is predominantly composed of silicon (61.00%) and iron (13.60%) oxides, while the cement contains mostly calcium (60.90%) and silicon (18.20%) oxides. These results are corroborated by the chemical mapping of the raw materials obtained through EDS analysis (Figure 4).

In the IOT samples, iron (Fe) is the predominant element, followed by silicon (Si) and aluminum (Al). In the reference sample, calcium (Ca) is present in the highest quantity, followed by silicon (Si) and aluminum (Al). For the GN samples, silicon (Si) is the dominant element, with smaller amounts of aluminum (Al) and iron (Fe).

Crystalline phases of IOT and GN are shown in Figure 5. IOT contains kaolinite, quartz, goethite, hematite and magnetite, whereas GN is composed of kaolinite, albite, biotite and quartz.

Mix design by the particle packing method

The optimal cement-to-sand ratios (1:1; 1:2; 1:3 and 1:4) were determined using the least squares method (LSM), as proposed by Garcia *et al.* (2022). Among the tested ratios, the 1:3 mixture exhibited the best performance compared to the theoretical values (Figure 6a), as indicated by the lowest LSM value. Based on this result, the 1:3 proportion (cement to sand) was adopted for subsequent tests. Silica fume contents of 25%, 30%, and 35% were evaluated to determine the ideal contents of the IOT and the GN, which were varied from 0% to 50% (Figure 6b). The silica fume range was selected due to its impact on workability and tendency to increase water demand. The convergence of the LSM curves for silica fume at 25%, 30%, and 35% indicated an optimal IOT content of 40%. This finding is consistent with the results reported by other authors (Almada *et al.*, 2022, 2023; Castro *et al.*, 2021). Despite the differences in particle size distribution between the IOT and the GN, no significant variation was observed in LSM values. Thus, the same IOT content (40%) was adopted for the GN samples.

Table 3 - Chemical composition of materials by FRX

Oxide	Silica fume	IOT	GN	Cement
Fe ₂ O ₃	13.60	69.90	3.72	3.08
SiO ₂	61.00	19.20	70.50	18.20
Al ₂ O ₃	11.30	3.46	14.30	4.37
CaO	3.44	0.22	3.18	60.90
MgO	1.86	0.10	1.60	0.60
TiO ₂	0.91	0.10	0.39	0.24
P ₂ O ₅	0.36	0.10	0.14	0.25
Na ₂ O	0.70	0.10	3.85	0.15
K ₂ O	2.31	---	2.85	0.68
MnO	0.26	0.15	0.05	0.07
SO ₃	---	---	---	3.96
LOI	5.27	5.75	0.89	6.62

Figure 4 - Chemical mapping (by EDS) of the materials: (a) IOT, (b) Ref., and (c) GN

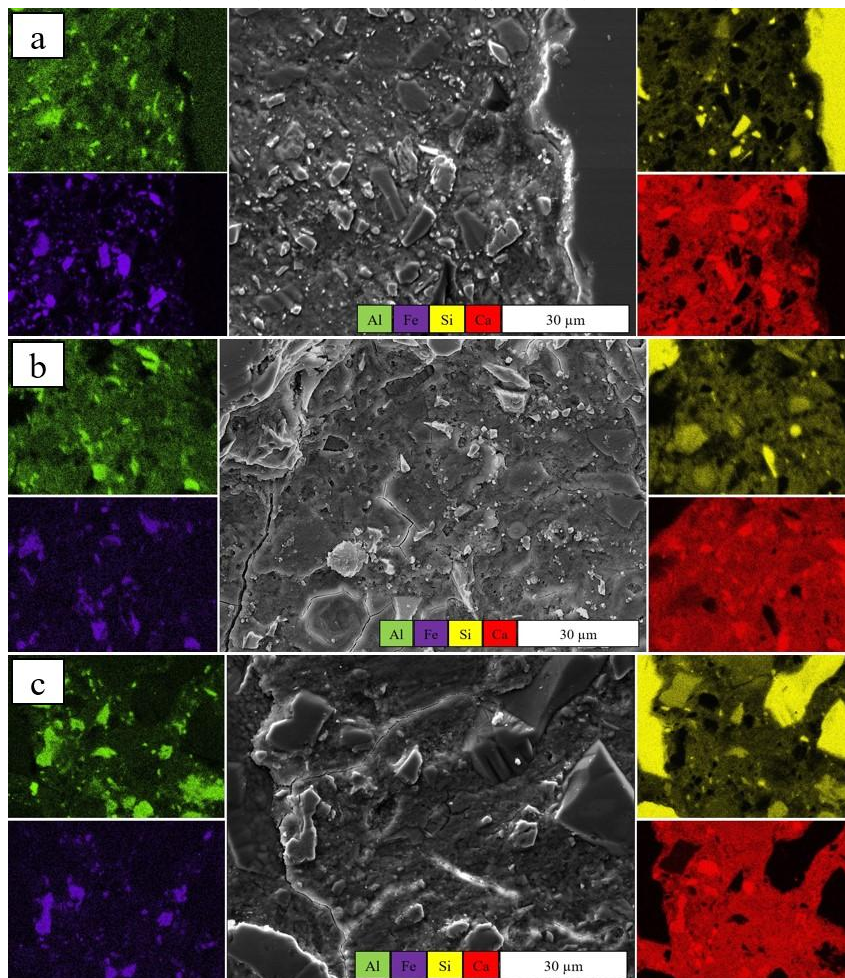


Figure 5 - X-ray diffraction (XRD) results of the studied waste materials: (a) IOT, (b) GN

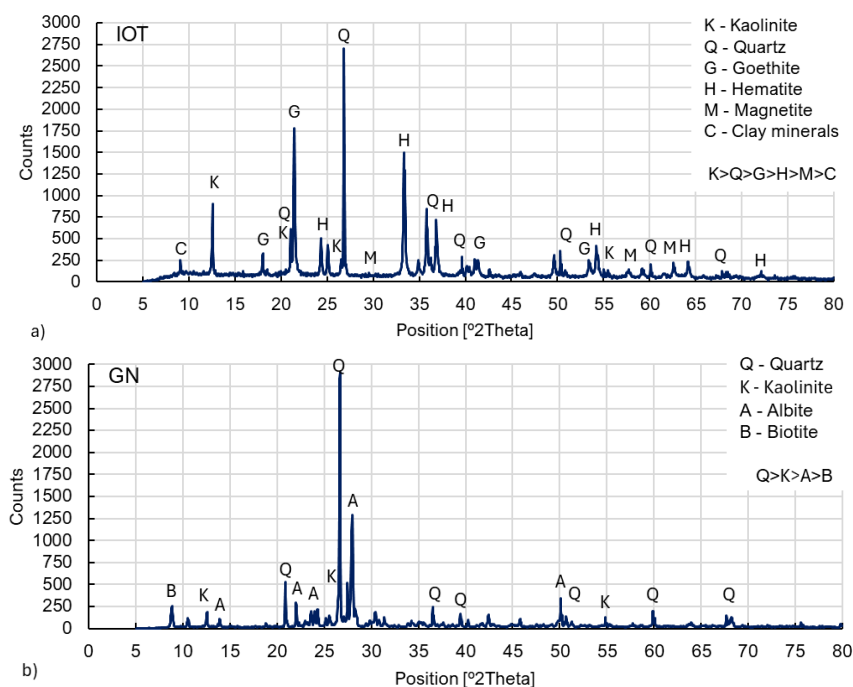
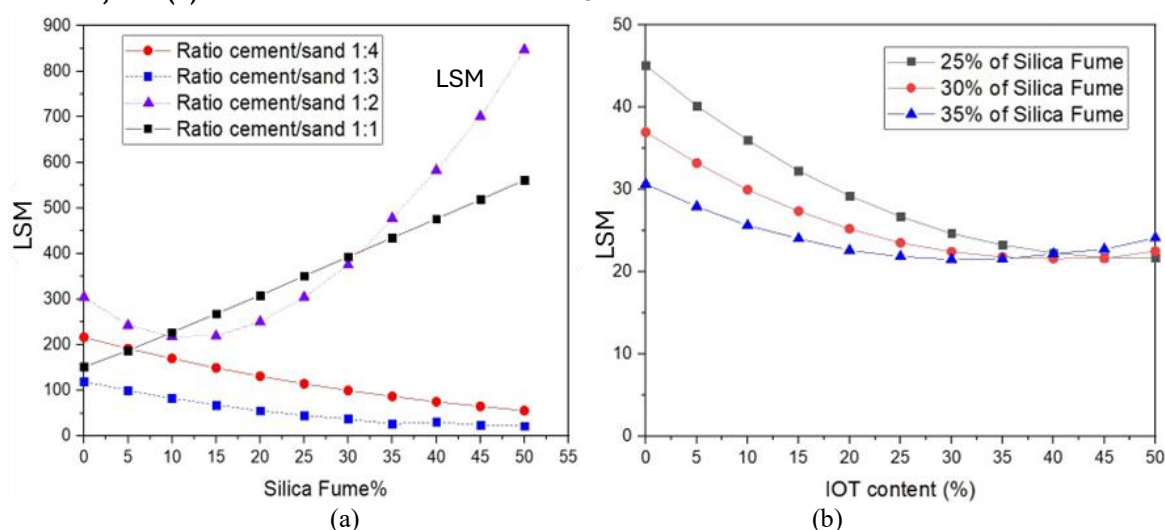


Figure 6 - Least Squares Method (LSM) results of the (a) cement to sand ratios with varied silica fume contents, and (b) silica fume contents with varied IOT contents



The EMMA software was used to define the theoretical particle-packing curve of the cementitious composite and to estimate the quantity of each raw material. After that, the mix design was adjusted experimentally to determine the water-to-cement ratio (w/c) and the superplasticizer content. The w/c was set at 0.375, and the superplasticizer dosage was adjusted to achieve a consistency of (230 ± 10) mm, measured in the flow table. The final proportions of the raw materials obtained from the experimental tests are presented in Table 4. Although the GN and the IOT have different particle size distribution, the optimal GN dosage was also approximately 40%, indicating that the relationship between density and particle size led to a convergence in the required amounts of these materials within the studied mixtures.

Physical and durability parameters

Figure 7 shows the open porosity results, all of which were below 4%, significantly lower than the typical range for conventional concrete (10 - 15%) (Marvila *et al.*, 2017). These results suggest the formation of a composite material with high-strength potential. Since the values are low, small variations can converge to large proportional variations - IOT (16.85% compared to Ref.) and GN (14.40% compared to Ref.). However, great similarities between the samples studied can be seen. Particularly at 180 days, only IOT specimen showed a significant increase (58%) in porosity, which may be associated with experimental errors or any unknown deleterious reaction or shrinkage of the sample. The low values of porosity and minimal results variability can be attributed to an effective particle packing effect (item 3.2), which distinguishes this study from others in the literature. Almada *et al.* (2022) showed the lowest value of open porosity was 13.0% for IOT samples (compared to 2.33% at 28 days in this research). The theoretical porosity also presented low values (0.09%) when compared to those reported by other authors (Almada *et al.*, 2022; Castro *et al.*, 2021), who found values close to 25%.

This observation (Figure 7) is further supported by a slight increase in the density of the samples, 9.87% for IOT and 7.29% for GN, when compared to the reference mixture. Although this increase could potentially lead to a higher self-weight in structural applications, the relatively small variation suggests the overall impact may be minimal. The higher density observed in IOT and GN composites may be attributed to the efficient particle packaging promoted by the dosing method.

When analyzing water absorption by immersion (Figure 8), the few existing pores (Figure 7) appear to be poorly interconnected (Figure 8). The packing effect led to a reduction in the quantity and size of pores (Figure 6). The GN mineral admixture resulted in maximum packing, with a 24.56% reduction in water absorption, while IOT resulted in reduction of only 11.50% in this property. All samples exhibited satisfactory results, mostly lower than those found in the literature: 24% (Almada *et al.*, 2022), 13% (Castro *et al.*, 2021) and 17% (Balestra *et al.*, 2020). Regarding the age of the tests, the results were generally consistent, with a notable exception in the IOT samples, which showed a 59% increase in water absorption. This suggests the presence of interconnected surface pores that contributed to increased porosity and water absorption. These pores appear to be relatively large, as they did not significantly influence the capillary absorption results.

Table 4 - Proportion of the raw materials of mixtures

Sample	Cement	Sand	Silica Fume	IOT	GN	Water	Superplasticizer
IOT	1.000	3.000	0.250	0.400	0.000	0.375	0.030
GN	1.000	3.000	0.250	0.000	0.400	0.375	0.030
Ref.	1.000	3.000	0.250	0.000	0.000	0.375	0.020

Figure 7 - Open porosity and density results of the samples

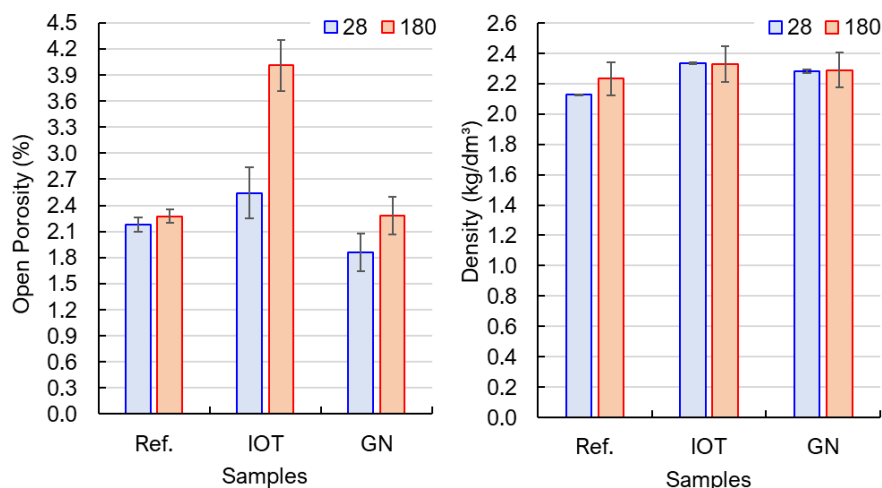
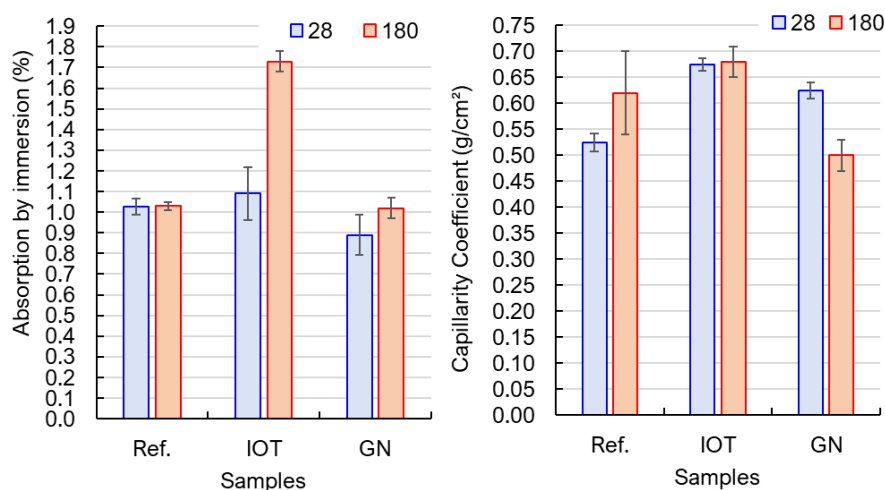


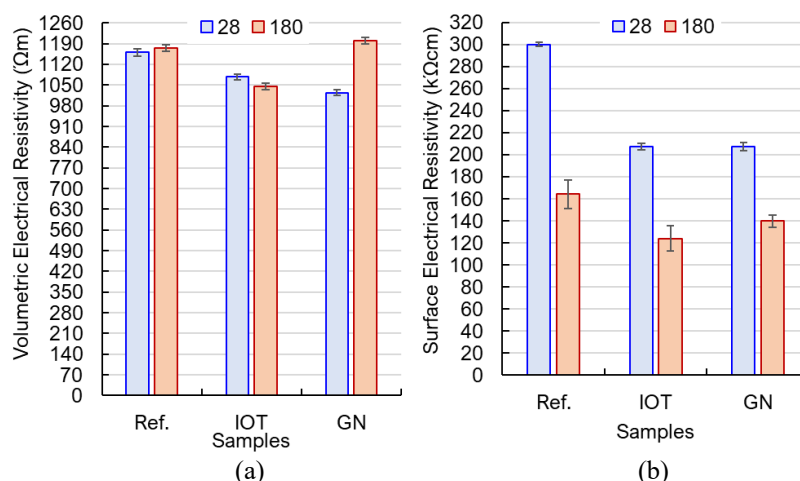
Figure 8 - Absorption by immersion and capillarity coefficient results



The capillarity coefficient can be an indicator for understanding and predicting the durability of mortars (Magalhães *et al.*, 2020). All results exhibited low values, indicating low pore connectivity, which may suggest an enhanced durability. The GN reduced capillary absorption by 20%, which may be associated with improved silica fume reactivity due to increased nucleation sites and the clogging open pores at advanced ages.

Figure 9a shows the results of volumetric electrical resistivity. This property is of great importance for evaluating durability (ASTM, 2019), as it can also be correlated with the probability of chloride penetration (Medeiros; Lima, 2016). Chloride penetration is considered high for resistivity values lower than 120 $\Omega \cdot m$; moderate between 120 $\Omega \cdot m$ and 210 $\Omega \cdot m$; low between 210 $\Omega \cdot m$ and 370 $\Omega \cdot m$; very low between 370 $\Omega \cdot m$ and 2,540 $\Omega \cdot m$; and insignificant for resistivity values greater than 2,540 $\Omega \cdot m$. The resistivity values obtained in the present study were 1,077 $\Omega \cdot m$ and 1,024 $\Omega \cdot m$ for IOT and GN samples, respectively, which are considered too low for chloride penetration (Medeiros; Lima, 2016). However, other authors (Almada *et al.*, 2022) reported much lower values for IOT composites (around 36 $\Omega \cdot m$), which may suggest a high probability to chloride penetration.

Figure 9 - Volumetric and surface electrical resistivity results



Results of surface electrical resistivity (Figure 9b) were satisfactory for all samples. At 28 days, both IOT and GN samples had similar values, around 207 kΩ.cm, suggesting a very low corrosion potential (Hornbostel; Larsen; Geiker, 2013). According to Balestra *et al.* (2020), corrosion potential in concrete is very high for resistivity values lower than 5 kΩ.cm; high between 5 kΩ.cm and 9 kΩ.cm; moderate between 9 kΩ.cm and 17 kΩ.cm; low between 17 kΩ.cm and 41 kΩ.cm; very low 41 kΩ.cm and 220 kΩ.cm; and insignificant for values greater than 220 kΩ.cm. However, compared to the reference samples, a decrease of approximately 30% was observed in samples with the IOT and the GN. This reduction may be associated with changes in water interaction at the surface of the samples, with increased water affinity in the IOT and GN mixtures. A significant drop was also observed between 28 and 180 days, with a 45% reduction for Ref., 40% for IOT and 33% for GN. Notably, the mineral admixture of IOT and GN resulted in a smaller reduction, highlighting their positive effect on the performance of these materials.

The adopted w/c ratio (0.375) may have also contributed to the satisfactory electrical resistivity result, as it is lower than the ratios used in other studies, such as a w/c of 0.50 (Almada *et al.*, 2022). Therefore, the lower the amount of water, the lower the porosity and its interconnections, resulting in a denser composite and greater electrical resistivity (Medeiros; Lima, 2016). Another reason for high electrical resistivity may be attributed to the mineral admixture of 25% of silica fume, which leads to pores refinement and reduced permeability.

Therefore, the results of surface and volumetric electrical resistivity indicate that both the IOT and GN composites exhibit adequate durability, evidenced by their very low susceptibility to chloride penetration and corrosion initiation. These findings are also supported by other durability indicators, such as open porosity, water absorption by immersion and density, which also demonstrated satisfactory performance.

Mechanical parameters

Results of compressive and flexural strengths are shown in Figure 10. They can be classified as high-strength materials, with compressive strength values of approximately 94.2 MPa for IOT samples and 98.0 MPa for GN samples. At 28 days, the compressive strength results for all three conditions are similar, indicating that the incorporation of IOT and GN did not significantly change the mechanical behavior. The high compressive strength in IOT and GN composites is associated with efficient particle packing and fine particle sizes. The results indicate that all composites fall within the classification of high-strength cementitious materials. This is particularly evident when compared to other studies involving IOT (Almada *et al.*, 2022, 2023), which reported compressive strength results of 48.30 MPa and 44.00 MPa, respectively. Regarding the age of the test, the Ref. sample showed the greatest mechanical gain with an increase of 14%, while IOT and GN showed slight increases of 3% and 7%, respectively. At 180 days, GN exceeded 100 MPa compressive strength.

There is a slight variation in the flexural strength by the mineral admixture of IOT and GN, resulting in increases of 2.69% and 10.32% compared to the Ref., respectively. This is due to improved bonding of waste particles within the cement matrix, where they act as nucleation sites and enhance the pozzolanic activity of silica fume. This contributes to better hydration in cementitious composites with a low w/c ratio (0.375). However, when analyzing strength development over time (from 28 to 180 days), the Ref. mix showed an increase of 12.73%, while IOT and GN composites exhibited slight reductions of 1.37% and 5.14%,

respectively. This suggests that strength gains in IOT and GN composites primarily occur within the first 28 days, with minimal variation thereafter. This demonstrates that nucleation points accelerate the reactions of silica fume (Fajardo; Souza; Santos, 2025).

Microstructure parameters

The quantity of pores of the composites at 28 days was determined by image analysis (Figure 11). It was obtained by the area of pores in relation to the total area of the sample (2D images). All samples had similar percentage of pores: Ref. (1.46%), IOT (1.49%) and GN (1.70%). The data obtained by image analysis followed the same trend as the values obtained by open porosity.

Ref. and IOT samples exhibited similar quantity of anhydrous phases, with 2.97% and 3.10%, respectively, while the GN sample presented a slightly higher value of 5.22%. However, it is important to note that, despite this small variation, all samples showed a high degree of hydration and a well-densified cement paste.

Figure 11 shows the thermogravimetric analysis results. The mass loss related to both calcium hydroxide (CH) and calcium carbonate was low in all samples. Although a difference is observed between the Ref. and GN samples, these variations in mass loss are not significant in the TGA analysis. Figure 12 shows BSE-SEM micrographs used to assess porosity of the interfacial transition zone (ITZ), particularly in the size range of 5 μm and 50 μm .

Figure 10 - Compressive and flexural strength results

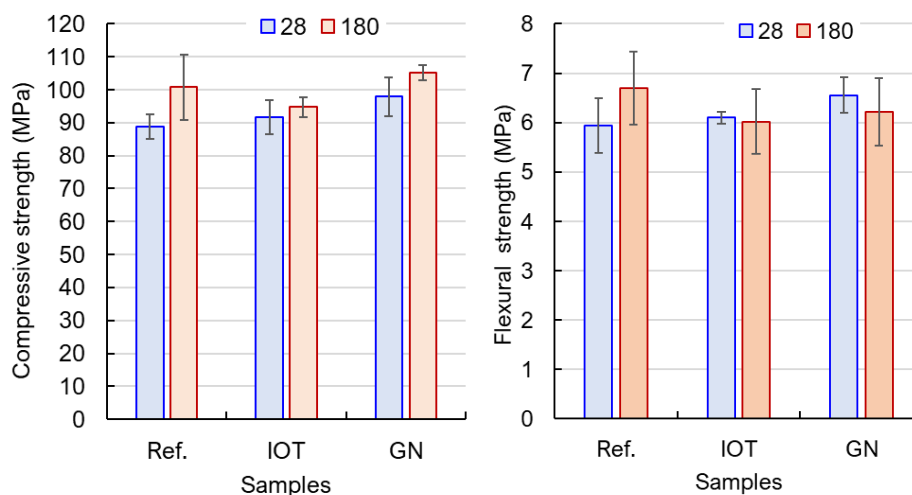


Figure 11 - Quantity of pores and anhydrous phase by SEM and calcium carbonate and hydroxide mass

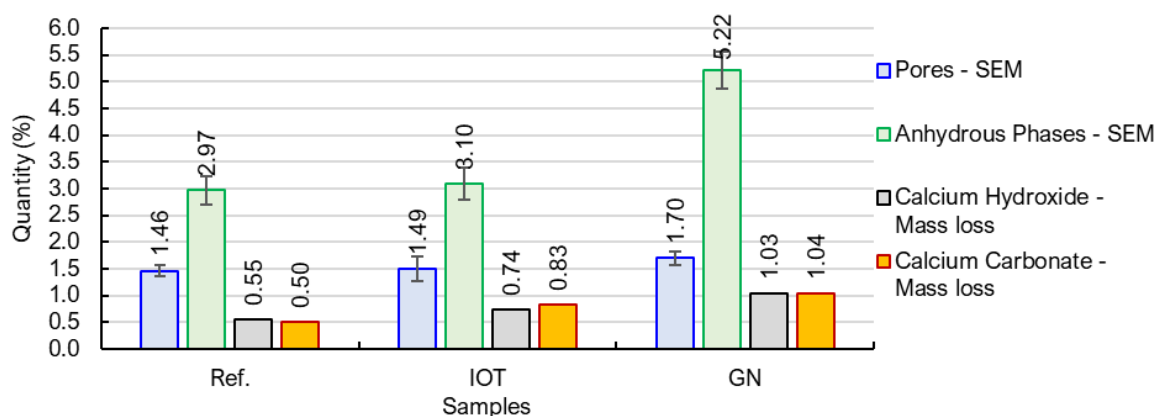
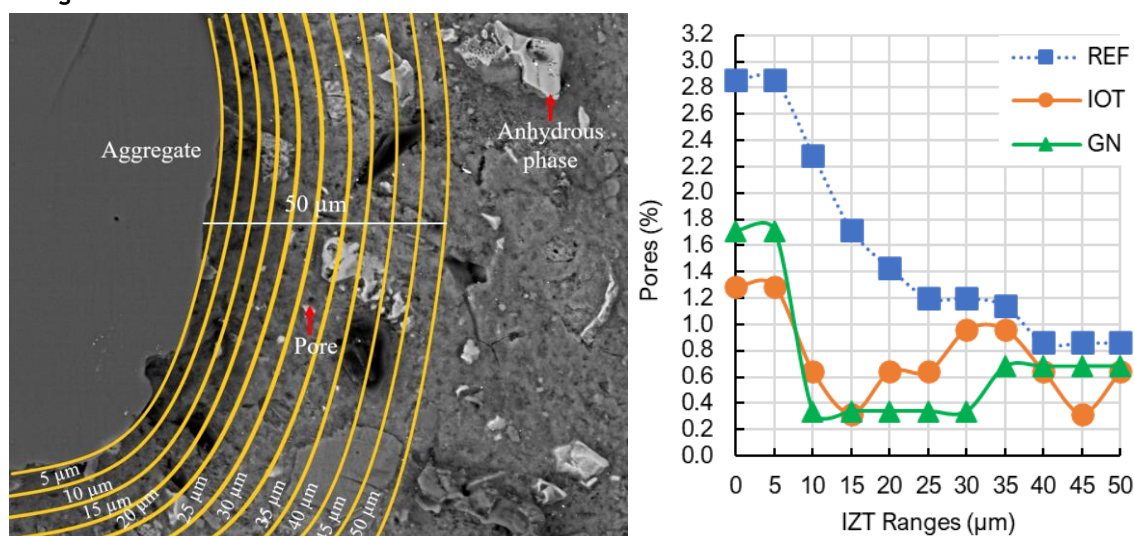


Figure 12 - Segmentation of Ref. sample to porosity analysis and development of porosity of samples throughout the ITZ



All composites presented the highest pore content closer to the aggregate (within the 5 μm range) and with a tendency to reduce up to the 50 μm range. The Ref. sample had the highest pore content, 2.86%, followed by GN (1.71%) and IOT (1.29) samples. Therefore, both the IOT and GN mineral admixture resulted in a denser ITZ microstructure, supporting the pore count results (Figure 12) and open porosity data (Figures 6 and 7). This effect may be attributed to enhanced particle packing, where the fine particles were also able to lodge close to ITZ, densifying this region. Their presence, associated with the nucleation effect, did not reduce the mechanical properties, as shown in Figure 8. In samples with IOT and GN, porosity is more evenly distributed within 5-10 μm range, while in the Ref. sample, this distribution occurs primarily in the 20-25 μm band. It can be seen that both mineral admixtures reduce the size of the interfacial transition zone, resulting in a denser, stronger, and more durable cementitious matrix (Almada *et al.*, 2022, 2023).

Conclusions

This paper evaluated high-strength cementitious composite with iron ore tailings (IOT) and gneiss powder (GN) as mineral admixture. Based on the experimental study, the following conclusions can be drawn:

- the physical characteristics (particle size of 4.7 μm , surface area of 35,133 m^2/g , and density of 3.85 g/cm^3) and chemical compositions (48% Fe_2O_3 and 21.20% SiO_2) of IOT and GN influence the performance of high-strength cementitious composites;
- the fine particles of IOT and GN, along with the effective packaging effect, resulted in highly densified composites with reduced porosity (less than 2.6% at 28 days);
- water absorption was reduced by the mineral admixture of IOT and GN due to the filler effect and decreased pore interconnectivity, as evidenced by low water absorption by immersion, low theoretical porosity, and low capillarity coefficient;
- both mineral admixtures improved the mechanical properties, with compressive strength exceeding 90 MPa, flexural tensile strength above 6 MPa, and increased durability. Surface and volumetric electrical resistivity values were higher than 47 $\text{k}\Omega\cdot\text{cm}$ and 370 $\Omega\cdot\text{m}$, respectively. These results are attributed to improved particle anchoring within the cement paste, enhanced pozzolanic activity of the silica fume due to nucleation sites provided by the IOT and GN, effective particle packing, and low w/c ratio (0.375); and
- microstructural analysis of the interfacial transition zone revealed low pore contents in the IOT and GN samples (1.29% and 1.71%, respectively) within the 5 μm range near the aggregate. Additionally, both wastes effectively reduced the thickness of this weaker zone by approximately half, concentrating porosity within the 5 to 10 μm range.

Therefore, by employing a mix design approach based on the particle packing method, it was possible to develop high-strength cementitious composites with excellent physical, mechanical and durability

performance. Furthermore, the study demonstrated the feasibility of producing high-strength composites through incorporation of IOT and GN waste materials.

References

- ALMADA, B. S. *et al.* Evaluation of the microstructure and micromechanics properties of structural mortars with addition of iron ore tailings. **Journal of Building Engineering**, v. 63, p. 1-17, 2023.
- ALMADA, B. S. *et al.* Study of mechanical, durability and microstructural properties of cementitious composite with addition of different iron ore tailings from Brazil. **Journal of Materials Research and Technology**, v. 18, p. 1947-1962, 2022.
- AMERICAN SOCIETY FOR TESTING AND MATERIALS. **C150**: standard specification for Portland Cement. West Conshohocken, 2024.
- AMERICAN SOCIETY FOR TESTING AND MATERIALS. **C215**: standard test method for fundamental transverse, longitudinal, and torsional resonant frequencies of concrete specimens. West Conshohocken, 2019.
- ASSOCIAÇÃO BRASILEIRA DE NORMAS TÉCNICAS. **NBR 13279**: argamassas aplicadas em paredes e tetos: determinação da resistência à flexão e à compressão na fase endurecida. Rio de Janeiro, 2005a.
- ASSOCIAÇÃO BRASILEIRA DE NORMAS TÉCNICAS. **NBR 7214**: areia padrão para ensaios de cimento: especificação. Rio de Janeiro, 2015.
- ASSOCIAÇÃO BRASILEIRA DE NORMAS TÉCNICAS. **NBR 7215**: cimento Portland: determinação da resistência à compressão de corpos de prova cilíndricos. Rio de Janeiro, 2019.
- ASSOCIAÇÃO BRASILEIRA DE NORMAS TÉCNICAS. **NBR 9778**: argamassa e concreto endurecidos: determinação da absorção, vazios e massa específica. Rio de Janeiro, 2005b.
- ASSOCIAÇÃO BRASILEIRA DE NORMAS TÉCNICAS. **NBR 9779**: argamassa e concreto endurecido: determinação da absorção de água por capilaridade. Rio de Janeiro, 2012.
- ASSOCIAÇÃO NACIONAL DAS ENTIDADES DE PRODUTORES DE AGREGADOS PARA CONSTRUÇÃO. **Mercado**. 2024. Available: <https://anepac.org.br/mercado/>. Acesso: 05 nov. 2024.
- BALESTRA, C. E. *et al.* Evaluation of chloride ion penetration through concrete surface electrical resistivity of field naturally degraded structures present in marine environment. **Construction and Building Materials**, v. 230, n. 116979, 2020.
- BEZERRA, C. G. *et al.* Feasibility of iron-rich ore tailing as supplementary cementitious material in cement pastes. **Construction and Building Materials**, v. 303, n. 124496, 2021.
- BRAZILIAN MINING INSTITUTE. **Information about the Brazilian mineral economy**. 2021. Available: <https://ibram.org.br/wp-content/uploads/2021/02/Economia-Mineral-Brasileira-IBRAM-2020.pdf>. Access: 01 may 2025.
- CANCIO, A.S. *et al.* Study of the reuse of iron ore tailing in cementitious compounds. **International Journal of Science and Engineering Investigations**, v.7, n. 77, p. 148–53, 2018.
- CARRASCO, E. V. M. *et al.* Characterization of mortars with iron ore tailings using destructive and nondestructive tests. **Construction and Building Materials**, v. 131, n. 30, p. 31–38, Jan. 2017.
- CARVALHO, J. M. F. *et al.* Influence of particle size-designed recycled mineral admixtures on the properties of cement-based composites. **Construction and Building Materials**, v. 272, n. 22, 2022.
- CASTRO, N. L. B. *et al.* Influence of addition contents of iron ore tailings on structural mortar. **Journal of Management and Sustainability**, v. 11, n. 1, p. 74, 2021.
- CHÁCARA D. M.; OLIVEIRA FILHO, W. L. Rheology of mine tailings deposits for dam break analyses. **REM - International Engineering Journal**, v. 74, n. 2, p. 235–243, 2021.
- CHEN, Z. *et al.* Utilization of gneiss coarse aggregate and steel slag fine aggregate in asphalt mixture. **Construction and Building Materials**, v. 93, p. 911–918, 2015.
- CHENG, Y. *et al.* Test Research on the Effects of Mechanochemically Activated iron tailings on the compressive strength of concrete. **Construction and Building Materials**, v. 118, n. 15, p. 164–70, 2016.

FAJARDO, A. A.; SOUZA, S. R.; SANTOS, W. J. High-performance structural mortars with the admixture of silica fume from steel waste. **Ambiente Construído**, Porto Alegre, v. 25, e138597, jan./dez. 2025.

GARCIA D. C. S. *et al.* Evaluating the effect of autoclave curing on the microstructure and compressive strength evaluation of a high strength concrete. **Materia**, v. 27, n. 2, e13201, 2022.

GIANNETTI, B. F. *et al.* Towards more sustainable social housing projects: recognizing the importance of using local resources. **Building and Environment**, v. 127, p. 187-203, 2018.

GU, X. *et al.* Hydration characteristics investigation of iron tailings blended ultra-high-performance concrete: the effects of mechanical activation and iron tailings content. **Journal of Building Engineering**, v. 45, n. 103459, 2022.

GUANG, Y.; DENG, Y.; WANG, J. Non-hydrothermal synthesis and characterization of MCM-41 mesoporous materials from iron ore tailing. **Ceramics International**, v. 40, n. 5, p. 7401-7406, 2014.

HORNBOSTEL, K.; LARSEN, C. K.; GEIKER, M. R. Relationship between concrete resistivity and corrosion rate: a literature review. **Cement and Concrete Composites**, v. 39, p. 60-72, 2013.

HUANG, X.; RANADE, R.; LI, V. C. Feasibility study of developing green ECC using iron ore tailings powder as cement replacement. **Journal of Materials in Civil Engineering**, v. 25, n. 7, p. 923-31, 2013.

LEÃO, R. B. S. *et al.* Mix design method for coating mixed mortar according to influence of the aggregate type and application environment conditions. **International Journal of Civil Engineering**, v. 22, p. 1061-1079, 2024.

LING, G. *et al.* Utilizing iron ore tailing as cementitious material for eco-friendly design of ultra-high-performance concrete (UHPC). **Materials**, Basel, v. 14, n. 8, 2021.

LIU, J. H. *et al.* Reconstruction of Broken Si-O-Si Bonds in Iron Ore Tailings (IOTs) in concrete. **International Journal of Minerals, Metallurgy and Materials**, v. 26, n. 10, p. 1329-1336, 2019.

LUO, L. *et al.* Preparation, characteristics and mechanisms of the composite sintered bricks produced from shale, sewage sludge, coal gangue powder and iron ore tailings. **Construction and Building Materials**, v. 232, n. 117250, 2020.

LV, X. *et al.* Environmental impact, durability performance, and interfacial transition zone of iron ore tailings utilized as dam concrete aggregates. **Journal of Cleaner Production**, v. 292, n. 126068, 2021.

MAGALHÃES, L. F. *et al.* Iron ore tailing as addition to partial replacement of Portland cement. **Materials Science Forum**, v. 930, p. 125-130, 2018.

MARVILA, M. T. *et al.* Estudo da capilaridade para argamassas de múltiplo uso, In: ABM ANNUAL CONGRESS, 72., São Paulo, 2017. **Anais [...]** São Paulo: Editora Blucher Preceding, 2017.

MEDEIROS, R. A.; LIMA, M. G. Electrical resistivity of unsaturated concrete using different types of cement. **Construction and Building Materials**, v. 107, p. 11-16, 2016.

MORAIS, C. F. *et al.* Thermal and mechanical analyses of colored mortars produced using Brazilian Iron Ore Tailings. **Construction and Building Materials**, v. 268, n. 121073, 2021.

NATIONAL MINING AGENCY. **Brazilian mineral yearbook: main metallic substances**. Brasília, 2021. Available: https://www.gov.br/anm/pt-br/centrais-de-conteudo/publicacoes/serie-estatisticas-e-economia-mineral/anuario-mineral/anuario-mineral-brasileiro/amb_2020_ano_base_2019_revisada2_28_09.pdf. Access: 03 may 2025.

PIRES, K. S. *et al.* Mineralogical characterization of Iron Ore Tailings from the quadrilatero ferífero, Brazil, by electronic quantitative mineralogy. **Materials Research**, v. 22, n. e20190194, 2019.

SCHANKOSKI, R. A. *et al.* Fresh and hardened properties of self-compacting concretes produced with diabase and gneiss quarry by-product powders as alternative fillers. **Construction and Building Materials**, v. 224, p. 659-670, 2019.

TORRES, A. J. *et al.* The influence of sugarcane bagasse ash on the microstructure of autoclaved cementitious material: comparative study with amorphous and crystalline silica. **Journal of Materials Research and Technology**, v.33, p. 1309-1321, 2024.

UNITED STATE GEOLOGICAL SURVEY. **National minerals information center: mineral commodity summaries**. 2021. Available: <https://pubs.er.usgs.gov/publication/mcs2021>. Access: 05 may 2025.

YANNICK, T. L. *et al.* Properties of waste gneiss powder used to design eco-friendly cement mortar. **JMST Advances**, v. 6, p. 1-21, 2024.

ZHANG, W. *et al.* Effects of iron ore tailings on the compressive strength and permeability of ultra-high-performance concrete. **Construction and Building Materials**, v. 260, n. 119917, 2020.

Acknowledgments

The authors acknowledge National Council for Scientific and Technological Development (CNPq - grants 304596/2022-1 and 409493/2023-6), Coordination for the Improvement of Higher Education Personnel (CAPES) and Minas Gerais Research Support Foundation (FAPEMIG - grants APQ-00584-21, APQ- 00062-22, APQ-06746-24, APQ-04155-23) for their financial support.

Declaração de Disponibilidade de Dados

Os dados de pesquisa só estão disponíveis mediante solicitação OU

Abner Araújo Fajardo

Formal analysis, Investigation, Validation, Writing - original draft, Writing - review + editing.

Mestrado em Construção Civil | Universidade Federal de Minas Gerais | Av. Presidente Antônio Carlos, 6627, Pampulha | Belo Horizonte - MG - Brazil | CEP 31270-901 | Tel.: (31) 3409-1809 | E-mail: fajardo.aabner@gmail.com

Sílvia Roberta Souza

Formal analysis, Investigation, Validation, Writing - original draft, Writing - review + editing.

Mestrado em Construção Civil | Universidade Federal de Minas Gerais | E-mail: roberta.souzar@hotmail.com

Dyala Fraga do Prado

Formal analysis, Investigation, Validation, Writing - original draft.

Graduação em Engenharia Civil | Universidade Federal de Minas Gerais | E-mail: dyala.prado@gmail.com

Jordana Gonçalves de Macedo

Formal analysis, Investigation, Validation, Writing - original draft.

Graduação em Engenharia Civil | Universidade Federal de Minas Gerais | E-mail: jordanagdmacedo@gmail.com

Vinicius Ferreira Lanna

Formal analysis, Investigation, Validation, Writing - original draft.

Graduação em Engenharia Civil | Universidade Federal de Minas Gerais | E-mail: viniciusfl@ufmg.br

Maria Teresa Paulino Aguiar

Formal analysis, Funding acquisition, Supervision, Methodology, Investigation, Validation, Writing - original draft, Writing - review + editing.

Departamento de Engenharia de Materiais e Construção | Universidade Federal de Minas Gerais | Av. Presidente Antônio Carlos, 6627, Pampulha | Belo Horizonte - MG - Brazil | CEP 31270-901 | Tel.: (31) 3409-1852 | E-mail: mtpaguiar@gmail.com

Dayana Cristina Silva Garcia

Formal analysis, Funding acquisition, Supervision, Methodology, Investigation, Validation, Writing - original draft, Writing - review + editing.

Departamento de Engenharia de Materiais e Construção | Universidade Federal de Minas Gerais | Tel.: (31) 3409-1964 | E-mail: dayanacsilvagarcia@gmail.com

Maria Teresa Gomes Barbosa

Formal analysis, Funding acquisition, Supervision, Methodology, Investigation, Validation, Writing - original draft, Writing - review + editing.

Departamento de Construção Civil | Universidade Federal de Juiz de Fora | Rua José Lourenço Kelmer, s/n, Campus Universitário, São Pedro | Juiz de Fora - MG - Brazil | CEP 36036-330 | Tel.: (32) 2102-3405 | E-mail: teresa.barbosa@engenharia.ufjf.br

Fernando do Couto Rosa Almeida

Formal analysis, Funding acquisition, Supervision, Methodology, Investigation, Validation, Writing - original draft, Writing - review + editing.

Departamento de Engenharia de Materiais e Construção | Universidade Federal de Minas Gerais | Tel.: (31) 3409-3558 | E-mail: fernandocralmeida@gmail.com

White José dos Santos

Formal analysis, Funding acquisition, Supervision, Methodology, Investigation, Validation, Writing - original draft, Writing - review + editing.

Departamento de Engenharia de Materiais e Construção | Universidade Federal de Minas Gerais | Tel.: (31) 3409-1809 | E-mail: white.santos@demc.ufmg.br

Editor-chefe: **Enedir Ghisi**

Editora convidada: **Luciani Somensi Lorenzi**

Ambiente Construído

Revista da Associação Nacional de Tecnologia do Ambiente Construído

Av. Osvaldo Aranha, 99 - 3º andar, Centro

Porto Alegre - RS - Brasil

CEP 90035-190

Telefone: +55 (51) 3308-4084

www.seer.ufrgs.br/ambienteconstruido

www.scielo.br/ac

E-mail: ambienteconstruido@ufrgs.br



This is an open-access article distributed under the terms of the Creative Commons Attribution License.